

THE COLD AND DUSTY CIRCUMSTELLAR MATTER AROUND FAST-EXPANDING TYPE IA SUPERNOVAE

XIAOFENG WANG^{1*}, JIA CHEN¹, LIFAN WANG^{2,3},
MAOKAI HU³, GAOBO XI¹, YI YANG^{4,2}, WENXIONG LI¹

Draft version October 30, 2018

ABSTRACT

Type Ia supernovae (SNe Ia) play key roles in revealing the accelerating expansion of the universe, but our knowledge about their progenitors is still very limited. Here we report the discovery of a rigid dichotomy in circumstellar (CS) environments around two subclasses of type Ia supernovae (SNe Ia) as defined by their distinct photospheric velocities. For the SNe Ia with high photospheric velocities (HV), we found a significant excess flux in blue light during 60-100 days past maximum, while this phenomenon is absent for SNe with normal photospheric velocity (Normal). This blue excess can be attributed to light echoes by circumstellar dust located at a distance of about $1-3 \times 10^{17}$ cm from the HV subclass. Moreover, we also found that the HV SNe Ia show systematically evolving Na I absorption line by performing a systematic search of variable Na I absorption lines in spectra of all SNe Ia, whereas this evolution is rarely seen in Normal ones. The evolving Na I absorption can be modeled in terms of photoionization model, with the location of the gas clouds at a distance of about 2×10^{17} cm, in striking agreement with the location of CS dust inferred from B-band light curve excess. These observations show clearly that the progenitors of HV and Normal subclasses are systematically different, suggesting that they are likely from single and double degenerate progenitor systems, respectively.

Subject headings: supernovae: general—supernovae: progenitors — supernovae: distance scale

1. INTRODUCTION

It is conventionally accepted that type Ia supernovae (SNe Ia) result from thermonuclear explosion of a carbon-oxygen (CO) white dwarf (Nomoto et al. 1997, Hillebrandt et al. 2000, Maoz 2014). Two popular scenarios are: merger-induced explosion of two white dwarfs (the so-called double degenerate (DD) scenario) and accretion-induced explosion of a massive WD with a non-degenerate companion (the so-called single degenerate (SD) scenario). Many progenitor classes have been proposed (Gilfanov et al. 2010, Wang & Han 2012, Maoz 2014), but observational evidences have not yet reached definitive conclusions on particular progenitor systems. The SD scenario is favored by the possible detections of circumstellar materials (CSM) around some SNe Ia through detections of strong ejecta-CSM interaction (Hamuy et al. 2003, Wang et al. 2004, Aldering et al. 2006, Silverman et al. 2013, Bochenek et al. 2018) or evolving narrow absorption lines possibly due to CSM (Patat et al. 2007, Blondin et al. 2009, Sternberg et al. 2011, Dilday et al. 2012), while there are also observational findings suggesting no companion signatures for some SNe Ia (Li et al. 2011a, Gonzalez et al. 2012, Schaefer et al. 2012, Olling et al. 2015). This may suggest that SNe Ia have multiple progenitor systems, as favored by the discovery that SNe Ia with different ejecta velocities originate from distinct birthplace environments (Wang et al. 2013).

Observationally, spectroscopically normal SNe Ia consists of $\sim 70\%$ of all SNe Ia (Branch et al. 1993, Li et al. 2011b) and can be categorized into high-velocity (HV) and normal-

velocity (NV) subclasses based on ejecta velocities inferred from the blueshifted Si II 6355 Å line (Wang et al. 2009). Compared to NV ones, HV SNe have systematically redder $B-V$ colors at maximum light and prefer abnormally low total to selective absorption R_V ratios (Wang et al. 2009). It is thus important to examine whether this difference arises from the intrinsic difference of the SN ejecta or from systematic difference in circumstellar (CS) and/or interstellar environments of the two groups. These issues may shed light on the elusive progenitor systems of SNe Ia.

The presence of CS dust can be tested by examining the behaviors of narrow interstellar absorption features. The interstellar sodium Na I doublet (D_1 5896 Å, D_2 5890 Å) is a good tracer of gas, dust and metals, and its strength is correlated with line-of-sight dust reddening (Munari et al. 1997, Pozanski et al. 2012, Phillips et al. 2013). Its evolution (or variation) and velocity structure can provide significant constraints on the presence and distance of CS dust around SNe Ia (Patat et al. 2007, Chugai 2008, Simon et al. 2009, Sternberg et al. 2011), while it is not clear why evolution or velocity structure of interstellar Na I lines exist in some SNe Ia but not in the others. On the other hand, the surrounding CS dust may also affect the light curves of SNe Ia as a result of light scattering by the nearby dust. This can be examined by inspecting light curves in the early nebular phase.

In this Letter, we conducted a systematic search for variable Na I absorption in low-resolution spectra of SNe Ia as well as an overall analysis of the behavior of their late-time light curves, with an attempt to constrain the dust environments around SNe Ia and hence the properties of their progenitors. This letter is organized as follows: in Section 2, we describe the dataset of SNe Ia used in our analysis. The results from interstellar Na absorptions and late-time light curves are presented in Section 3. Discussions and conclusions are given in Section 4.

¹ Physics Department and Tsinghua Center for Astrophysics, Tsinghua University, Beijing 100084, China; wang_xf@mail.tsinghua.edu.cn

² Mitchell Institute for Fundamental Physics and Astronomy, Texas A&M University, College Station, TX 77843, USA

³ Purple Mountain Observatory, Nanjing, 210008, Jiangsu, China

⁴ Department of Particle Physics and Astrophysics, Weizmann Institute of Science, Rehovot 76100, Israel

2. DATASET

The spectral sample used to measure the Na absorption features in SNe Ia are primarily from the Center for Astrophysics (CfA) Supernova Program, the Carnegie Supernova Project (CSP). The former sample contains 2603 spectra of 462 nearby SNe Ia (Blondin et al. 2012), and most (94%) of which were obtained with the FAST spectrograph on the 1.5 m telescope at the Fred Lawrence Whipple Observatory (FLWO). The latter dataset contains 604 spectra of 93 SNe Ia (Folatelli et al. 2013), which were mainly obtained with the 2.5 m du Pont Telescope at Las Campanas Observatory. All of the spectra were reduced in a consistent way and have a typical resolution of 6-7 Å, providing the largest homogeneous spectroscopic dataset of SNe Ia. We also used the spectra from the Berkeley Supernova Program (BSP, Silverman et al. 2012), consisting of 1298 spectra for 582 SNe Ia, to get further classifications of our SN Ia sample and measure the Na absorptions whenever necessary. The spectral phases were obtained with respect to the B -band maximum light, based on the published light curves of CfA (Riess et al. 1999, Jha et al. 2006, Hicken et al. 2009, Hicken et al. 2012), Lick Observatory Supernova Survey (LOSS, Ganeshalingam et al. 2010), and Carnegie Supernova Project (Contreras et al. 2010, Stritzinger et al. 2011). The light-curve parameters, including the peak magnitudes, the $B_{max} - V_{max}$ colors at the maximum light, and the post-maximum decline rates $\Delta m_{15}(B)$ are either taken from the above literatures or fit by ourselves. The measurement results and relevant photometric parameters for each SN sample are listed in Table 1.

To eliminate the effects from noise spikes on the continuum determination of Na I absorption doublet, we smoothed the observed spectra in the range of 5850~5950 Å (after corrections for the redshift of host galaxies) using the gaussian smoothing technique. The smoothed spectra are then used to find the local flux maximum and hence define the pseudo-continuum. The definition of pseudo-continuum and hence the calculations of the EW are automatic for our SN sample, but we also double-checked the integration limits by eyes to make sure that they are reasonably determined. For a few SNe whose spectra suffering from improper wavelength calibration and/or motion of the SNe relative to the galaxy center, we adjusted their integration limit manually. As the Na ID absorption of some SNe Ia is found to show temporal evolution within one week from the maximum light (see also Figure 2), the EW of each SN is taken as a weighted mean of the results obtained at $t \sim 10$ -30 days after the maximum light when multi-epoch spectra are available.

Table 1 lists the relevant parameters of our SN Ia sample, and the meaning of each column is as follows: Column (1), SN name; Column (2), the SN Ia subtype based on the Si II velocity at around the maximum light (Wang et al. 2009); (3), Si II velocity measured from Si II 6355 absorption in the near-maximum-light spectra; Column (4), $\Delta m_{15}(B)$, the B -band magnitude decline rate in 15 days from the maximum (Phillips 1993); Column (5), $B_{max} - V_{max}$ color at the maximum light, corrected for the Galactic reddening; Column (6), the weighted mean value of the equivalent width (EW) of Na I absorption over the period $10 < t < 30$ days whenever possible; Column (7), the B -band magnitude decline in the first 60 days after the B -band maximum; Column (8), the V -band magnitude decline in the first 60 days after the B -band maximum; Column (9), References.

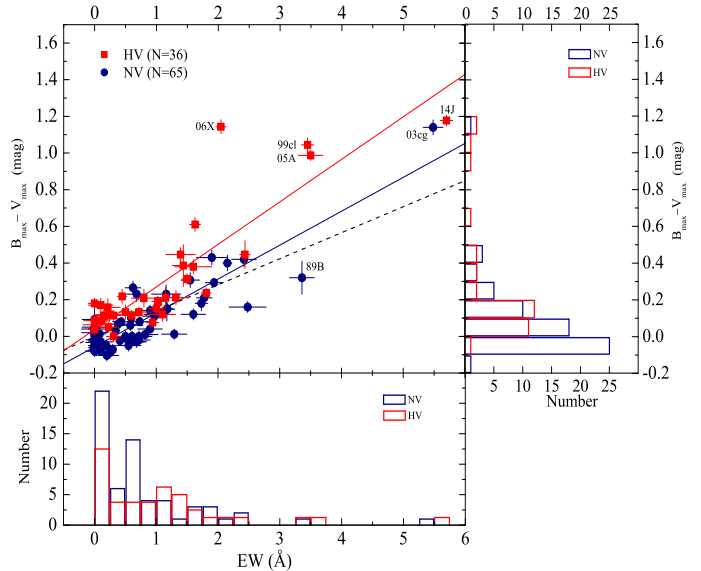


FIG. 1.— Relation between absorption strength (expressed as equivalent width) of interstellar sodium lines in spectra of SNe Ia and the corresponding values of their $B_{max} - V_{max}$ colors. The "HV" subgroup (red squares) represents the SNe Ia with larger Si II velocity at B -band maximum light, i.e., $v_{Si II}^0 \geq 12,000$ km s $^{-1}$, while the "NV" subgroup (blue circles) denotes those with $v_{Si II}^0 < 12,000$ km s $^{-1}$. The red and blue lines represent the best-fit linear relationship to the HV and NV SNe Ia, respectively, while the dashed, black line shows the relationship inferred from the Na absorption and reddening due to the Milky Way. SN 2006X was not included in the fit due to the saturation of the Na I lines (Patat et al. 2007). The plot is then projected onto the two side panels where a histogram is displayed for each SN Ia subclass in each of the dimensions.

3. RESULTS

3.1. Narrow Na I Absorption Features

Figure 1 shows the $B - V$ colors at the maximum light versus the EWs of the Na ID absorption due to the host galaxies. Foreground Galactic reddening corrections have been removed from the observed colors. The $B_{max} - V_{max}$ color has been usually used as an indicator of reddening (Phillips et al. 1999, Wang et al. 2009), though some SNe Ia may have peculiar colors.

As can be readily seen, the correlation between $B_{max} - V_{max}$ color and strength of Na absorption is apparent for the HV and NV subclasses, with stronger Na I D absorptions corresponding to redder colors (and hence larger reddening). However, these two subclasses of SNe Ia show noticeable differences in the distribution of their $B_{max} - V_{max}$ colors and the Na ID EWs. A two-dimensional Kolmogoroff-Smirnoff (KS) test gives a probability of 0.15% that they have statistically identical Na ID EW and color distribution. Examining the EW of Na I absorption and the $B_{max} - V_{max}$ color separately yields a respective probability of 5.9% and 0.003% that the two subclasses have the same parent distribution. The mean $B_{max} - V_{max}$ colors estimated for these two subclasses are 0.26 mag (HV) and 0.08 mag (NV), respectively, while the mean Na ID EWs are 1.1 Å (HV) and 0.7 Å (NV), respectively. In general, the HV subclass have redder colors and stronger Na ID absorption lines, and the fraction found with EWs > 1.0 is as high as 48.6% (versus 23.8% for the NV counterparts). These results indicate that the HV SNe Ia suffer significantly stronger reddening on average than the NV ones; the intrinsic color of HV SNe Ia may not necessarily be redder than their NV counterparts despite of their observed red color contrary to previous

studies (i.e., Foley & Kasen 2011).

Applying a linear fit to the $EW - (B_{max} - V_{max})$ relation for the HV and NV SNe Ia separately, we found that the former subclass have a larger slope of 0.231 ± 0.016 , while the slope for the latter is 0.173 ± 0.011 . This difference may be explained with incomplete recombination of the ionized Na (see Figure 2) and/or time evolving scattering of the SN photons by the surrounding dust (Wang 2005).

It is important to further constrain the location of the dust that gives rise to the excess extinction and the time varying Na ID absorption in HV SNe Ia. If the SN exploded near a dusty shell/slab, we may expect variable Na I absorptions in SN spectra due to photoionization effect (Chugai et al. 2008, Patat et al. 2011). The strength of the absorption may then be correlated with the rise and fall of the supernova luminosity. The trend that the Na ID absorptions become stronger after maximum light has already been reported for a few SNe Ia such as SN 2006X (Patat et al. 2007), SN 2007le (Simon et al. 2009), SN 1999cl (Blondin et al. 2009), but the decrease in strength of Na I absorption expected shortly after explosion was never observed in SNe Ia.

To investigate the EW variations, we consider all objects having at least three-epochs of spectroscopic data within ~ 1 month from the maximum light. Applying a $3\text{-}\sigma$ detection cut and a minimum EW variation of 0.5 \AA to the CfA and CSP data, we get a sample of 19 SNe Ia showing prominent Na ID variations. Table 2 lists the relevant parameters of this sample showing variable Na absorptions. Of this 19 SNe Ia, there are 12 HV and 3 NV SNe Ia, with a fraction of 63.2% and 15.8%, respectively. This sample increases to 26 when applying a $2\text{-}\sigma$ cut, which contains 14 HV SNe Ia (53.8%) and 7 NV SNe Ia (26.9%). The above analysis indicates that the varying of Na ID absorptions are statistically associated with the HV subclass. The probability of a chance coincidence is less than 0.1%. Variable sodium features have already been detected in the high-resolution spectra of SN 2006X and SN 2007le, and low-resolution spectra of SN 1999cl. It is gratifying to note that the evolutions of their Na ID line are nicely recovered in these low resolution data.

The Na ID absorption of some representative SNe Ia with significant time evolution is shown in Figure 2. The plot suggests that the Na ID line of these objects generally follow a qualitatively similar evolutionary trend. At early times the strength of the Na ID absorption was found to decrease with time, as is clearly seen in SN 2002bo, SN 2002dj, SN 2006X, and perhaps in SN 2002cd. Such an evolution can be attributed to photoionization of neutral Na by the UV photons of supernovae (Borkowski et al. 2009). After the declining phase, the Na absorption strength undergoes a rising stage lasting for about 10 days and remains at constant level after that. The overall evolution looks like a "square-root" sign, which can be well explained with a model of Na ID photoionization and recombination in CS dust (see solid curves in Figure 2) as discussed below.

In our model calculation, we adopted a symmetric CS dust shell with a temperature of about 100 K (Kamp et al. 2001, Douvion et al. 2001, Johansson et al. 2013). The intensity of the UV photons accounting for the photoionization of Na I was obtained using spectral template of SNe Ia (Nugent et al. 2002, Hsiao et al. 2007). The SN distance to the dust shell (R_S), the electron density in the dust shell (n_e), and the fraction of CS component of Na I are free parameters, which are related to ionization fraction and recombination time scale (or

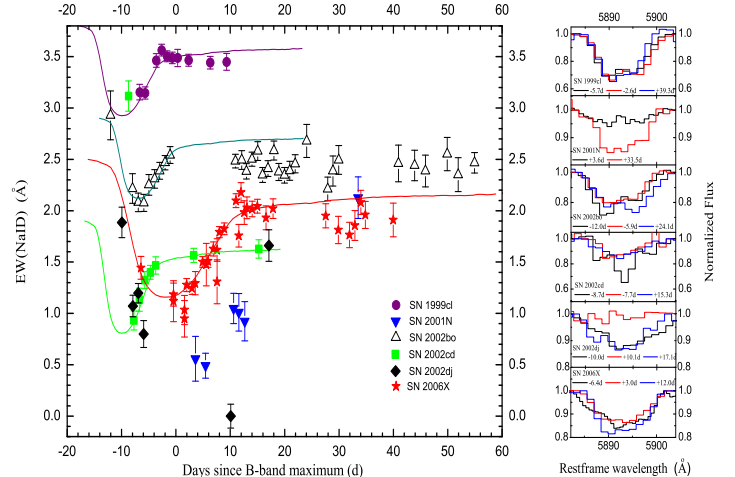


FIG. 2.— Temporal evolution of the equivalent width of Na I doublet for type Ia supernovae (SNe Ia). Left: Variable Na absorptions detected in some well-observed objects such as SNe 1999cl, 2001N, 2002bo, 2002cd, 2002dj, and 2006X. Note that all of the 6 SNe Ia shown in the plot belong to the "HV" subclass. Overplotted are the curves derived with a model of Na I photoionization and recombination in CS dust. Right: the continuum-normalized Na ID profile shown at several epochs for some well-observed HV SNe Ia. The black and red lines represent the earlier and near-maximum-light phase spectra, respectively, while the blue ones show the profile in the recombination phase.

final recombination fraction) of Na ID. One can see that the overall evolution of Na ID absorption seen in some HV SNe Ia is similar to that predicted by a simple CS shell model. By comparing with the model curves, typical values of $R_S \sim 0.1$ pc (3×10^{17} cm) and $n_e \sim 5 \times 10^7 \text{ cm}^{-3}$ can be found for the subsample showing evolving Na ID absorptions. Of the sample listed in Table 2, the reddening towards SN 2001N may be dominated by the CS dust as Na seems to be nearly completely ionized around the peak luminosity; and the dust shell may be located at a distance with $R_S < 0.1$ pc. The longer recombination time scale ($\gtrsim 30$ days) suggests that the density of the CS material is quite low, e.g., $n_e (\lesssim 10^7 \text{ cm}^{-3})$. Note that estimates of the above parameters may suffer large uncertainties from the difficulties in distinguishing the CS component from the component of Na ID absorption in these low-resolution spectra. Moreover, it is also difficult to determine accurately the total amount of neutral Na due to line saturation. Nevertheless, the above analysis indicates that the excess reddening of HV SNe Ia is related to the CS dust.

3.2. Late-time Light Curves

The presence of CS dust can be also tested by examining the behaviors of late-time light curves of SNe Ia. This is because some of the SN photons will be scattered by surrounding dust and arrive at the observer with a time delay (Wang et al. 1996, Wang et al. 2005, Patat et al. 2006). The delayed photons can be seen as a light echo (LE) and may contribute to the observed light curves in the early nebular phase, especially in blue bands. To examine the difference of the late-time light curves for our sample of SNe Ia, we measured the magnitude decline within 60 days from the B - and V -band maximum light, as defined by $\Delta m_{60}(B)$ and $\Delta m_{15}(V)$, respectively. These two quantities are obtained by applying a linear fit to the observed data spanning the phase from $t \sim +40$ days to $t \sim 100$ days, as listed in Table 1.

Figure 3 shows the BV -band light curves and the $B-V$ color

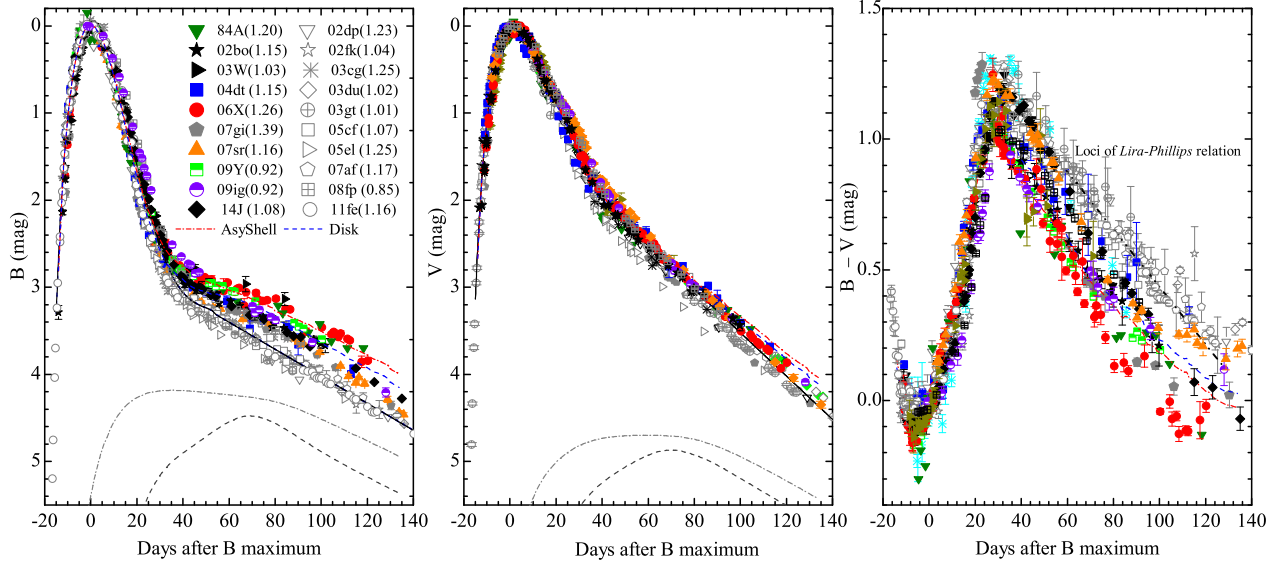


FIG. 3.— The B - (left panel), V -band light (middle panel) and $B-V$ color (right panel) curves of some well-observed SNe Ia (see Table 1 for the references of the data), with the curves being all normalized to the corresponding values at around the maximum light. The filled and semi-filled symbols the HV SNe Ia, and the open symbols denote the NV ones. SNe Ia of these two subclasses exhibit large differences in B band and $B-V$ colors 40 days after the maximum brightness. The black solid lines indicate the mean light curves of NV subsample. The extra emission by scattering of SN light on CS materials of an asymmetric shell and a disk structure, at a distance of $\sim 1-3 \times 10^{17}$ cm, are shown with the gray dash-dotted line and dashed line, respectively. The resultant light curves by including contributions of CS scattering are indicated by the red dash-dotted line (for an asymmetric shell) and blue dashed line (for a disk configuration), respectively. The dash-dot-dotted line shows the best-fit to the $B-V$ color curves of NV SNe Ia using the *Lira-Phillips* relation (Phillips et al. 1999), with the non-reddening loci being shifted redwards by 0.15 mag. During 40 days $< t < 100$ days, the color curves of most HV SNe Ia are apparently bluer than those of normal SNe Ia, following a slope much steeper than the *Lira-Phillips* relation.

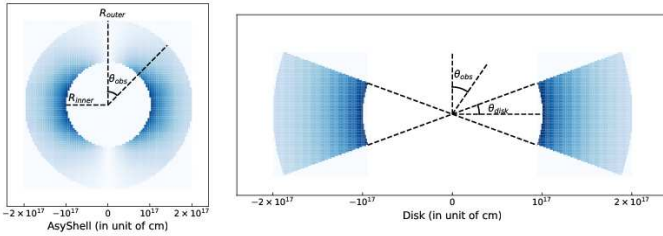


FIG. 4.— An illustration of the vertical planes of two different structures of CS dust, the asymmetric shell (a, left panel) and the disk (b, right panel). The vertical dashed lines show the symmetry axes of the two dust distribution. θ_{obs} shows the direction to the observer. The structures are rotationally symmetric with respect to the vertical dashed lines. The boundaries of the CSM are identified by the inner radius (R_{inner}), and outer radius (R_{outer}). The gray scale indicates the number density of the dust grains. The dust density decreases inversely with radius squared in both cases. For (a), the azimuth density dependence follows $\sin^2 \theta$, with θ being the angle to the symmetry axis.

curves for some well-observed SNe Ia. Although these SNe Ia have similar light curves in early phases, they show remarkable scatter in the B -band from $t \sim 40$ to 100 days after the peak. For instance, the B -band magnitude measured at $t \sim 60$ days from the peak can differ by over 0.5 mag in the B band (see Fig 3(a)). Such a late-time discrepancy is much smaller in the V band (see Fig 3(b)), which leads to an apparently bluer $B-V$ color for the HV SNe Ia relative to the NV objects, as shown in the right panel of Figure 3.

The extra light seen in the B band could be due to the scattering of SN light by the nearby CS dust, which can be quantitatively modeled for any given geometric configurations. In our models of dust scattering, we consider two structures of CS dust, an asymmetric shell (AsyShell) and a disk configuration, as seen in Figure 4. These two structures could be formed by the stellar wind and angular momentum transfer

from the companion, respectively. For simplicity, Rayleigh scattering is assumed in the calculations. We carried out these calculations assuming other scattering properties but will defer the discussion to a future paper (Hu et al. 2019 in prep.). To match the observed B - and V -band light curves of our HV sample, the CS dust is required to have an inner radius of $R_{inner} \sim 1 \times 10^{17}$ cm and an outer radius of $R_{outer} \sim 3 \times 10^{17}$ cm for most of our HV sample, with the opening angle (θ_{disk}) of 20° for the disk structure and optical depth (τ) of 0.8 and 0.5 for the disk and asymmetric shell, respectively. The number density along the radial direction is assumed to be inversely proportional to the distance squared as in the case of stellar wind ejection. The exact distance of the CS dust layer to any specific SN may be constrained by the duration of the brighter tails.

The modeled light/color curves, obtained by taking the mean light curves of NV SNe Ia as input of light scattering and assuming an aspheric dusty shell and a dusty disk at a distances between $1-3 \times 10^{17}$ cm, are overplotted in Figure 3. It is remarkable that the model light curves agree with the observed light/color scatter seen at 40-100 days after optical maximum. Note that the color measurements at these dates correspond to those used in the *Lira-Phillips* relation (Phillips et al. 1999) for color excess estimates of SNe Ia. This agreement is encouraging and is suggestive of the validity of these models and is in agreement with the presence of CS dust around SNe Ia. Moreover, the distance of the CS dust inferred from modeling of the late-time light curve is in strikingly consistent with that derived from the photoionization calculations presented in §3.1.

As more luminous SNe Ia tend to have brighter tails with slower decay rates, it is thus necessary to examine whether the excess emission seen in the tail light curves of HV SNe

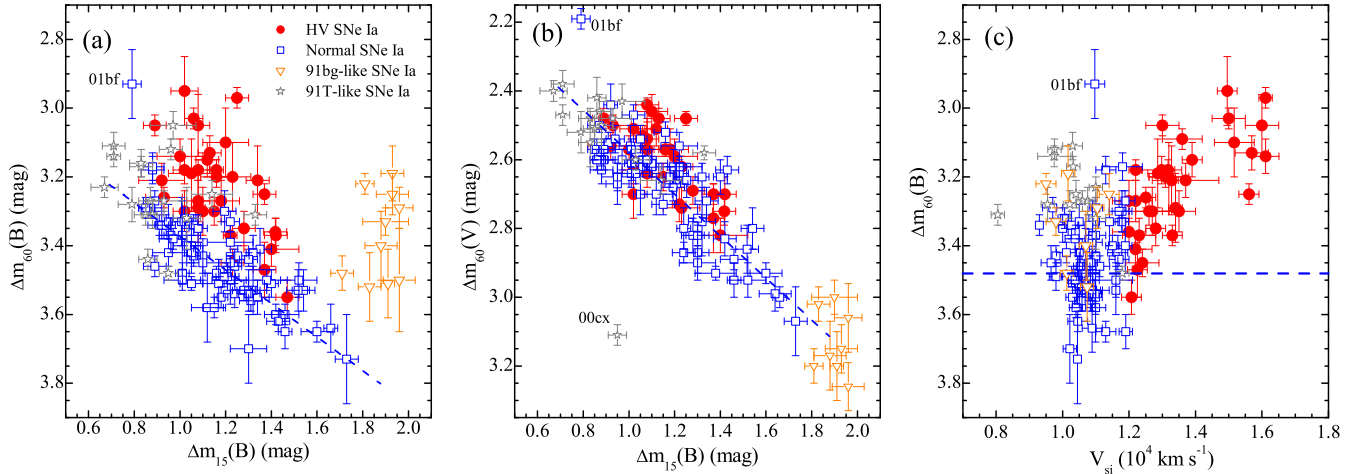


FIG. 5.— **a, b.** Tail brightness of SNe Ia, measured as magnitude decline at $t \sim +60$ days from the peaks of B - and V -band light curves, versus the luminosity indicator of SNe Ia $\Delta m_{15}(B)$ that is measured as the magnitude decline within the first 15 days after the B -band maximum (Phillips et al. 1993). **c.** A plot of the B -band tail brightness as a function of Si II velocity obtained around B -band maximum light. The subclasses of HV, NV, spectroscopically peculiar ones like SN 1991T and SN 1991bg SNe are shown by blue open squares, red dots, gray stars, and orange triangles, respectively. The blue dashed line in each panel represents the best linear fit for the NV subsample.

Ia is partially due to that they have intrinsically high luminosity. We plot the measured values of Δm_{60} as a function of the corresponding $\Delta m_{15}(B)$ for our sample in Figure 5, where one can see that the tail brightness does show a significant correlation with the decline rate in both B and V bands for the NV sample of SNe Ia. While this correlation shows large scatter in the B band for the HV subsample, with the measured $\Delta m_{60}(B)$ being systematically smaller than that of the NV ones at a given $\Delta m_{15}(B)$. This comparison further confirms that the excess emission in the blue band is not intrinsic to the HV SNe Ia. Instead, we found that the $\Delta m_{60}(B)$ shows a strong positive correlation with the Si II 6355 velocity measured around the maximum light, as shown in Fig 5(c). This indicates that the origin of the larger expanding velocity might be closely related to the formation of dusty environments around SNe Ia.

4. DISCUSSIONS AND CONCLUSIONS

The formation of CSM around an SN progenitor is a direct consequence of its progenitor evolution. The CSM can be ejected continuously similar to stellar winds, or episodically similar to nova shell ejections. Typical blueshift in the Na I lines of SNe Ia is $\sim 100 \text{ km s}^{-1}$ according to a statistical study using high-resolution spectra of 35 SNe Ia (Sternberg et al. 2011). The velocity and distance of the CS dust inferred here for HV SNe Ia suggest that they may have symbiotic nova progenitors, similar to RS Ophiuchi (Patat et al. 2011). Theoretical expectations for the fraction of SNe Ia from the symbiotic progenitor channel are ~ 1 to 30% (Lu et al. 2009), which is consistent with the birthrate of HV subclass, with a fraction of about 15-20% of all SNe Ia (Li et al. 2011b, Pan et al. 2015). For such a system, the fast-expanding nova shell (with a velocity of a few thousands of km s^{-1}) ejected from recurrent nova outbursts will be slowed down by the slow-moving stellar wind blown from the companion star, i.e., a red giant. Such an interaction process can create a large evacuated region around the SN progenitor and form a CS shell with a velocity of $\sim 100 \text{ km s}^{-1}$ at a distance ranging from 10^{15} cm to 10^{18} cm , consistent with the estimates for the HV sample. The extension and distance of the CS dust from the progenitor are likely related to the accretion rate, period of recurrent nova, and the time lag between the explosion and mass loss before

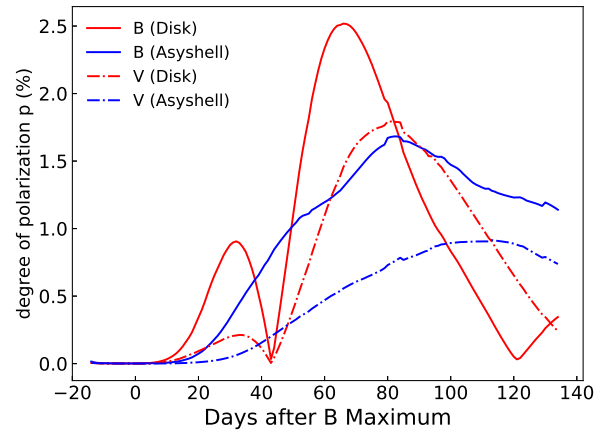


FIG. 6.— The predicted time-evolution of the polarization in the B - (solid line) and V -band (dot-dashed line) at a viewing angle of 30 degrees for the asymmetric shell. The blue curves show the polarization inferred from the asymmetric shell, while the red ones represent case for the disk structure.

explosion.

The distribution of the CS dust derived for the HV SNe Ia is typically around 10^{17} cm according to the above analysis, which is too compact to be spatially resolvable at extragalactic distances. The progenitors of SNe Ia involve binaries with one or two degenerate stars, the dust ejected from such systems may be naturally asymmetric. Polarimetry study of such compact light echos is able to map the geometric structures of the CSM and set observational constraints on the progenitor systems. We remark that the asymmetric dust distribution naturally leads to polarized radiation at late times when the scattered light is the strongest, corresponding to about 60-90 days after optical maximum, as shown in Figure 6. The absolute level of the degree of polarization is sensitive to the assumed geometric structure. Although only the SNe with highly asymmetric CS dust shells close to being edge-on are expected to produce strong polarization, the detection of such polarized signal and its evolution can be a prime evidence for the presence of the CS matter around the SNe (Wang et al. 1996). Unfortunately, existing polarimetry data are mostly taken around optical maximum (Wang & Wheeler 2008). In-

deed, recent deep HST imaging polarimetry of SN 2014J taken on day 277 after maximum reveals an abnormal polarization signal that can be identified with a light echo from a dust lump of at least $2 \times 10^{-6} M_{\odot}$, located at a distance of 5×10^{17} cm (Yang et al. 2018). More polarimetry at late epochs coupled with photometric monitoring holds the key to unlock the mystery concerning the CSM around SN Ia progenitors.

Our studies demonstrate that the HV SNe Ia are associated with the CS dust, which is in accordance with the detection of systematically blueshifted velocity structure (or outflow) in the Na I lines of SNe Ia having high Si II velocity (Sternberg et al. 2011). There are several additional evidences favoring that the HV subclass may originate from single degenerate progenitor system. For example, a significant ultraviolet excess is possibly detected in SN 2004dt and SN 2009gi (Wang et al. 2012, Foley et al. 2013), which is expected from the collision between ejecta and a larger companion such as a massive MS star or a red giant star (Kasen 2010). Moreover, there is a tendency that unburned carbon (i.e., C II 6580Å) is detected in the earlier spectra of NV SNe Ia (Parrent et al. 2011, Blondin et al. 2012, Silverman et al. 2012) but not in the HV SNe Ia. Recent studies also indicate that these two subclasses of SNe Ia also show significant differences in the velocity distribution of outer-layer oxygen and silicon (Zhao et al. 2016). These results are in line with the idea that SNe Ia with different ejecta velocities have different progenitor systems and /or explosion mechanisms. Combining with the results from the evolving narrow interstellar Na I absorptions and the late-time light curves presented in this report, we conclude that SNe Ia with fast expanding ejecta arise from progenitor systems with a red giant companion.

5. ACKNOWLEDGMENTS

This work is supported by the National Natural Science Foundation of China (NSFC grants 11325313, and 11633002), and the National Program on Key Research and Development Project (grant no. 2016YFA0400803). The work of L.W. is supported by NSF grant AST-1817099. This research has made use of the CfA Supernova Archive, which is funded in part by the National Science Foundation through grant AST 0907903. This research has also made use of the supernova archives from the Carnegie Supernova Project and the Berkeley Supernova Program, which are also funded in part by the US National Science Foundation.

TABLE 1
SUMMARY OF CLASSIFICATION, SPECTROSCOPIC AND PHOTOMETRIC PROPERTIES OF THE SN Ia SAMPLE

SN name	SN type	$v_{Si II}^0$ $\times 10^4 \text{ km s}^{-1}$	$\Delta m_{15}(B)$ (mag)	$B_{max} - V_{max}$ (mag)	EW (\AA)	$\Delta m_{60}(B)$ (mag)	$\Delta m_{60}(V)$ (mag)	Ref.*
SN 1984A	HV	1.47(04)	1.22(10)	0.16(09)	...	3.10(10)	2.59(05)	1
SN 1989B	NV	1.05(03)	1.35(05)	0.32(09)	3.36(10)	3.41(06)	...	2
SN 1994M	HV	1.24(02)	1.47(06)	0.10(04)	0.22(20)	3,4
SN 1994ae	NV	1.11(03)	0.89(05)	-0.05(04)	0.29(05)	3.46(03)	2.60(03)	3,4
SN 1995D	NV	1.01(02)	1.01(03)	0.01(03)	0.33(09)	3.32(03)	2.47(03)	3,4
SN 1996X	NV	1.13(03)	1.30(05)	-0.01(03)	0.00(10)	3.55(05)	2.72(04)	3,4
SN 1996bo	HV	1.23(05)	1.31(06)	0.36(04)	1.60(30)	3,4
SN 1997E	NV	1.18(03)	1.42(05)	0.05(03)	0.00(20)	3.60(03)	2.83(05)	3,4
SN 1997bp	HV	1.57(05)	1.11(03)	0.21(03)	1.81(10)	3.13(05)	2.48(03)	3,4
...

Note: The uncertainties shown in the brackets are 1σ , in units of 0.01 mag for $\Delta m_{15}(B)$, $B_{max} - V_{max}$, $\Delta m_{60}(B)$, and $\Delta m_{60}(V)$, and in units of 0.01 \AA for EW of Na I D absorption.

* 1= Barbon et al. 1989; 2 = Barbon et al. 1990; 3 = Matheson et al. 2008; 4 = Riess et al. 1999

TABLE 2
CANDIDATES OF TYPE IA SUPERNOVAE WITH VARIABLE
NA ID ABSORPTION FEATURES

SN name	$\Delta EW(\text{\AA})^a$	$\Delta EW/\sigma^b$	Number ^c	Type
SN 1997bp	0.66	3.5	13	HV
SN 1997bq	0.96	4.7	8	HV
SN 1998V	0.54	3.1	3	NV
SN 1999cl	1.07	5.0	11	HV
SN 1999dq	0.73	3.8	21	91T
SN 2000fa	1.20	4.5	4	HV
SN 2001br	1.27	4.4	4	HV
SN 2001N	1.64	6.9	6	HV
SN 2002bf	1.38	4.7	4	HV
SN 2002bo	0.85	3.4	31	HV
SN 2002cd	2.19	12.5	9	HV
SN 2002dj	1.89	10.0	6	HV
SN 2003ep	2.23	10.6	3	...
SN 2005cc	2.71	9.6	4	02cx
SN 2005hf	1.10	3.9	6	Pec
SN 2006N	1.02	4.1	7	NV
SN 2006X	0.93	8.2	21	HV
SN 2007le	0.67	4.0	25	HV
SN 2008C	1.27	6.5	5	NV

^a The maximum variation of the equivalent width (EW) measured from the Na I absorption in the spectra of SNe Ia.

^b The confidence that the SNe Ia show variable Na ID absorption, obtained by dividing the maximum variation of EW over the uncertainty in the measurement.

^c The number of the spectra used in the analysis.

REFERENCES

- Aldering, G., et al. 2006, *ApJ*, 650, 510
 Barbon, R., et al. 1989, *A&A*, 220, 83
 Barbon, R., et al. 1990, *A&A*, 237, 79
 Blondin, S., et al. 2009, *ApJ*, 693, 207
 Blondin, S., et al. 2012, *AJ*, 143, 126
 Bochenek, C. D., et al. 2018, *MNRAS*, 473, 336
 Borkowski, K. J., Blondin, J. M., Reynolds, S. P. 2009, *ApJ*, 699, L64
 Branch, D., Fisher, A., & Nugent, P. 1993, *AJ*, 106, 2383
 Contreras, C. et al. 2010, *AJ*, 139, 519
 Chugai, N. N. 2008, *Astronomy Letters*, 34, 389
 Dilday, B., et al. 2012, *Science*, 337, 942
 Douvion, T., Lagage, P. O., Cesarsky, C. J. et al. 2001, *A&A*, 373, 281
 Folatelli, G., et al. 2010, *AJ*, 139, 120
 Folatelli, G., et al. 2013, *ApJ*, 773, 53
 Foley, R. J. & Kasen, D. 2011, *ApJ*, 729, 55
 Foley, R. J. & Kirshner, R. P. 2013, *ApJ*, 769, L1
 Ganeshalingam, M., et al. 2010, *ApJS*, 190, 418
 Gilfanov, M. & Bogdán, Á. 2010, *Nature*, 463, 924
 González Hernández, J. I., et al. 2012, *Nature*, 489, 533
 Hamuy, M., et al. 2003, *Nature*, 424, 651
 Hicken, M. et al. 2009, *ApJ*, 700, 331
 Hicken, M., et al. 2012, *ApJS*, 200, 12
 Hillebrandt, W. & Niemeyer, J. C. 2000, *ARA&A*, 38, 191
 Hsiao, E., et al. 2007, *ApJ*, 663, 1187
 Hu, M. K., et al. 2019, in preparations
 Jha S., et al. 2006, *ApJ*, 527, 131
 Johansson, J., Amanullah, R., Goobar, A. 2013, *MNRAS*, 431, 43
 Kamp, I., Van Zadelhoff, G. J. 2001, *A&A*, 373, 641
 Kasen, D. 2010, *ApJ*, 708, 1025
 Li, W., et al. 2011a, *Nature*, 480, 348
 Li, W., et al. 2011b, *MNRAS*, 412, 1441
 Lu, G., et al. 2009, *MNRAS*, 396, 1086
 Maoz, D., Mannucci, F., & Nelemans, G. 2014, *ARA&A*, 52, 107
 Matheson, T., et al. 2008, *AJ*, 135, 1598
 Munari, U. & Zwitter, T. 1997, *A&A*, 318, 269
 Nomoto, K., Iwamoto, K., & Kishimoto, N. 1997, *Science*, 276, 1378
 Nugent, P., Kim, A., Perlmutter, S. 2002, *PASP*, 114, 803
 Olling, R. P. et al. 2015, *Nature*, 521, 332
 Pan, Y. C., et al. 2015, *MNRAS*, 446, 354
 Parrent, J. T., et al. 2011, *ApJ*, 732, 30
 Patat, F., et al. 2007, *Science*, 317, 924
 Patat, F., et al. 2011, *A&A*, 530, A63
 Phillips, M. M. 1993, *ApJ*, 413, L105
 Phillips, M. M., et al. 1999, *AJ*, 118, 1766
 Phillips, M. M., et al. 2013, *ApJ*, 779, 38
 Pozanski, D., et al. 2012, *MNRAS*, 426, 1465
 Riess, A. G., et al. 1999, *AJ*, 117, 707
 Riess, A. G. 2016, *ApJ*, 826, 56
 Schaefer, B. E., & Pagnotta, A. 2012, *Nature*, 481, 164
 Schlafly, E., F. & Finkbeiner, D. P. 2011, *ApJ*, 737, 103
 Silverman, J., et al. 2012, *MNRAS*, 425, 1917
 Silverman, J. M. & Filippenko, A. V. 2012, *MNRAS*, 425, 1917
 Silverman, J. M., et al. 2013, *ApJ*, 772, 125
 Simon, J. D., et al. 2009, *ApJ*, 702, 1157
 Sternberg, A., et al. 2011, *Science*, 333, 856
 Stritzinger, M. D., et al. 2011, *AJ*, 142, 156
 Verner, D. A. & Ferland, G. J. 1996a, *ApJ*, 465, 487
 Verner, D. A. & Ferland, G. J. 1996b, *ApJS*, 103, 467
 Wang, B. & Han, Z. 2012, *New Astronomy*, 56, 122
 Wang, L. & Wheeler, J. C. 1996, *ApJ*, 462, L27
 Wang, L., et al. 2004, *ApJ*, 604, L53
 Wang, L. 2005, *ApJ*, 635, L33
 Wang, L. & Wheeler, J. C. 2008, *ARA&A*, 46, 433
 Wang, X., et al. 2009, *ApJ*, 699, L139
 Wang, X., et al. 2012, *ApJ*, 749, 126
 Wang, X., Wang, L., Filippenko, A. V., Zhang, T., Zhao, X. 2013, *Science*, 340, 170
 Yang, Y., et al. 2018, *ApJ*, 854, 55
 Zhao, X., et al. 2016, *ApJ*, 826, 211